

On the Discriminability of Self-Supervised Representation Learning

Zeen Song, Wenwen Qiang, Changwen Zheng, Fuchun Sun, *Fellow, IEEE*, and Hui Xiong, *Fellow, IEEE*

Abstract—Self-supervised learning (SSL) has recently achieved significant success in downstream visual tasks. However, a notable gap still exists between SSL and supervised learning (SL), especially in complex downstream tasks. In this paper, we show that the features learned by SSL methods suffer from the crowding problem, where features of different classes are not distinctly separated, and features within the same class exhibit large intra-class variance. In contrast, SL ensures a clear separation between classes. We analyze this phenomenon and conclude that SSL objectives do not constrain the relationships between different samples and their augmentations. Our theoretical analysis delves into how SSL objectives fail to enforce the necessary constraints between samples and their augmentations, leading to poor performance in complex tasks. We provide a theoretical framework showing that the performance gap between SSL and SL mainly stems from the inability of SSL methods to capture the aggregation of similar augmentations and the separation of dissimilar augmentations. To address this issue, we propose a learnable regulator called Dynamic Semantic Adjuster (DSA). DSA aggregates and separates samples in the feature space while being robust to outliers. Through extensive empirical evaluations on multiple benchmark datasets, we demonstrate the superiority of DSA in enhancing feature aggregation and separation, ultimately closing the performance gap between SSL and SL.

Index Terms—self-supervised learning, representation learning, generalization bound.

I. INTRODUCTION

LEARNING discriminative feature representations in the absence of supervised signals has long been a prominent and widely explored research area in machine learning. Recently, self-supervised learning (SSL) has garnered significant attention due to its remarkable performance on various downstream tasks, including image classification [1], object detection [2], semantic segmentation and transfer learning [3], [4], [5].

Despite the continuous improvement in SSL performance through both augmentation-based and reconstruction-based approaches [1], [6], [7], [8], [9], a notable gap persists between SSL and supervised learning (SL), especially in tasks that require fine-grained discrimination. Understanding the underlying reasons for this gap remains an ongoing challenge.

Z. Song, W. Qiang, and C. Zheng are with the University of Chinese Academy of Sciences, Beijing, China. They are also with the Science & Technology on Integrated Information System Laboratory, Institute of Software Chinese Academy of Sciences, Beijing, China. E-mail: songzeen, lingyu, hujie, qiangwenwen, changwen@iscas.ac.cn. Z. Song and L. Si have contributed equally to this work.

F. Sun is with the Science & Technology on Integrated Information System Laboratory, Department of Computer Science and Technology, Tsinghua University, Beijing, China. E-mail: fcsun@tsinghua.edu.cn.

H. Xiong is with the Hong Kong University of Science and Technology, China. E-mail: xionghui@ust.hk.

To delve deeper into this issue, we conduct a series of toy experiments to illustrate the fundamental differences in the data characteristics learned by supervised and self-supervised methods. Specifically, we present a comparative analysis of five well-known SSL methods: SimCLR [1], BYOL [2], Barlow Twins [3], SwAV [10], and MAE [8]. For comparison, we also visualize the features learned by a supervised method.

The visualization of features learned by these methods on the ImageNet dataset [11] is shown in Fig. 1. From Fig. 1(a) to 1(f), we observe that features obtained by both SSL and supervised learning methods exhibit clustering characteristics, meaning points of the same class are grouped together. However, SSL methods display a large intra-class variance, which causes points at the edges of different classes to overlap, a phenomenon we refer to as the **crowding problem**. In contrast, supervised learning methods not only produce fine-grained intra-class features but also maintain clear separation between different classes.

We further interpret the observations mentioned earlier from both empirical and theoretical perspectives. For empirical analysis, we find that SSL methods lack a specific component in their objective function that explores the relationships between different samples. In contrast, supervised methods leverage annotation information to encourage the clustering of samples from the same class and the separation of samples from different classes in the feature space. For theoretical analysis, we demonstrate that minimizing intra-class variance and maximizing inter-class distance reduces the error risk in supervised learning. Based on these findings, we conclude that the performance gap between supervised learning and SSL methods may be attributed to the SSL methods' limited exploration of the dynamics between samples. Specifically, the objective function of SSL methods lacks a term that constrains points of similar semantics to be closer and points of dissimilar semantics to be further apart in the feature space. These insights provide valuable guidance for designing more effective regularization methods to close the performance gap between SSL and supervised learning.

Inspired by this analysis, we propose a novel method called "Dynamic Semantic Adjuster" (DSA) that can be seamlessly integrated into existing SSL methods as a learnable regulator. DSA consists of two main modules: the arranging module and the scoring module. The arranging module aggregates similar samples while effectively distinguishing dissimilar samples in the feature space using a learnable regulator matrix. However, due to the poor performance of the feature extractor in the initial stages of training, the regulator matrix may be inaccurate, leading to incorrect aggregation and separation. To address

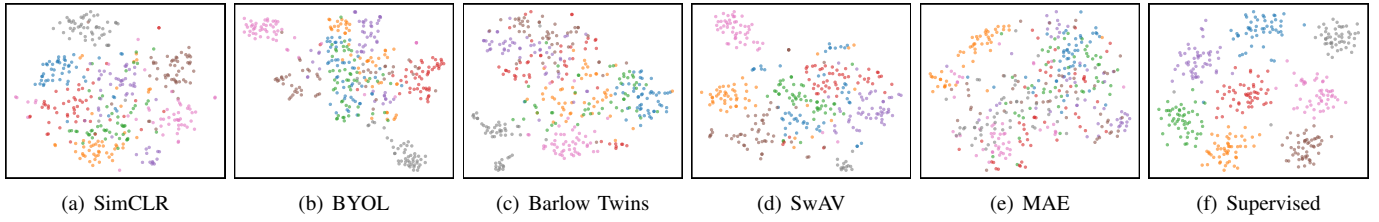


Fig. 1. Data distribution visualization based on 8 random classes of the test set of ImageNet in the feature space. (a) - (e) corresponds to the visualization results of the self-supervised method while (f) corresponds to the visualization results of the supervised method. We can observe that the **crowding problem** is present in SimCLR, BYOL, Barlow Twins, SwAV, and MAE.

this, we propose the scoring module, which aims to ensure that the regulator matrix preserves the local structure of the input sample space. This enhancement allows the matrix to more effectively explore similarity and dissimilarity in the early stages of training. Additionally, the scoring module ensures that the proposed contrastive learning method remains robust against outliers.

The main contributions are summarized as:

- We show for the first time that contrastive learning suffers from the crowding problem. We empirically analyze that the cause of the crowding problem is absence of a term in the objective function of contrastive learning that can explore relationships between augmentations generated from samples of different ancestors.
- We provide a theoretical analysis to demonstrate that the performance gap between contrastive learning and supervised learning primarily stems from the inability of contrastive learning methods to effectively capture the aggregation and separation between augmentations that are generated by samples of different ancestors.
- We propose a novel method called "Dynamic Semantic Adjuster" (DSA), which can make points of the same class cluster and points of different classes separate from each other. Notably, our method is insensitive to outliers and can be seamlessly integrated into existing contrastive learning models, facilitating its practical applicability.
- We provide empirical evaluations to substantiate the efficacy of the proposed DSA in improving the performance of various state-of-the-art contrastive learning methods.

II. RELATED WORK

In this section, we briefly review the SSL methods, especially those that also aim to analyze the discriminability of SSL. We also review the SSL methods most relevant to our work and highlight the differences between these methods and ours.

Self-Supervised learning. According to different learning paradigms, the SSL methods can be categorized into two classes, namely the augmentation-based methods and reconstruction-based methods.

Augmentation based.

The core idea behind augmentation-based methods is to create different views of a single sample through data augmentation while simultaneously making the representations of these different views more similar [12]. One of the most successful augmentation-based methods is SimCLR [1], which utilizes the

InfoNCE loss to group views from the same sample and repel views from different samples. One of the main drawbacks of SimCLR is the requirement for a large number of negative samples, i.e., views from different samples. Without sufficient negative samples, the problem of collapse can occur, where the shared representation ignores the input and remains constant. To address this limitation, negative-free methods are proposed. Recent methods such as BYOL [2], SimSiam [13], and DINO [6] have shown that collapse can be avoided within a knowledge distillation framework. Another line of negative-free methods, such as Barlow Twins [3], W-MSE [14], and VICReg [7], propose to prevent collapse by maximizing the information content of the embeddings.

Reconstruction based. Reconstruction-based SSL methods attempt to learn useful representations by reconstructing the original samples. Traditionally, an autoencoder takes the whole sample as input, feeds it into the encoder to obtain the latent representation, and then reconstructs the sample with a decoder. Variants of autoencoders, such as denoising autoencoders and variational autoencoders [15], have been adopted for self-supervised learning. Recently, inspired by the success of mask modeling in natural language processing, the reconstruction method with mask modeling has gained significant attention. Specifically, BEiT [16] and masked autoencoder (MAE) [8] randomly mask the contents of visual samples and aim to reconstruct the whole sample using only the unmasked parts.

We demonstrate in Section III that current SSL methods share a unified objective and our proposed DSA is a plug-and-play module that can be integrated with any SSL methods.

Discriminability Analysis. Discriminability refers to the easiness of separating feature representations from different categories. The concept of learning discriminative representations was first introduced by Linear Discriminant Analysis (LDA) [17], which aims to find a projection into a lower-dimensional space that maximizes the separation between multiple classes while retaining as much class-discriminatory information as possible. Various studies have investigated discriminability in the context of SSL methods. For example, Saunshi et al. [18] connect the SSL objective with supervised downstream error through instance discrimination. Chen et al. [19] proposed quantifying discriminability in SSL using the min-max distance ratio. In our research, we theoretically demonstrate that the downstream classification error risk is bounded by intra-class variance and inter-class difference, highlighting that the discriminability of feature representations significantly impacts downstream performance.

SSL with Clustering.

Clustering aims to group semantically similar samples. Traditionally, this unsupervised learning algorithm has been extensively used for small-scale, low-dimensional unlabeled data [20]. In recent years, several studies have integrated clustering algorithms with deep neural networks [21], [22], [23]. Our research introduces a learnable regulator designed to aggregate similar samples while distinguishing dissimilar ones, thus positioning our approach as a form of clustering. Other methods that combine SSL with clustering include SwAV [10], PCL [24], and NaCl [25]. These methods typically use a K-means-like paradigm, treating the number of centroids as a hyper-parameter. **Since we do not know the real number of classes during the training phase, samples of different classes may be clustered together and samples of the same class may be clustered near different class centroids. Therefore, crowding problem can also occur. In contrast, our method does not require a predefined number of clusters, instead grouping similar samples in an online manner. Furthermore, our DSA approach not only clusters similar samples but also separates dissimilar ones.**

III. PRELIMINARIES

In this section, we first present a unified framework for SSL methods and briefly introduce prominent SSL approaches, including SimCLR [1], BYOL [2], Barlow Twins [3], and Masked Autoencoder [8].

Formally, given a minibatch of training data denoted as $X_{tr} = \{x_i\}_{i=1}^N$, where x_i represents the i -th sample and N denotes the number of samples in the minibatch, the augmentation-based methods apply random data augmentations (e.g., random crop) to transform a random sample x_i into two augmented views x_i^1 and x_i^2 . Similarly, the reconstruction-based methods apply a random mask to the sample x_i , creating two masked views x_i^1 and x_i^2 . The augmented dataset is denoted as $X_{tr}^{aug} = \{x_1^1, x_1^2, \dots, x_N^1, x_N^2\}$. The samples in X_{tr} are considered as the ancestors of the samples in X_{tr}^{aug} . The augmented dataset X_{tr}^{aug} is then fed into the feature extractor f to obtain their feature representations, i.e., $r_i^l = f(x_i^l)$, where $i \in \{1, \dots, N\}$ and $l \in \{1, 2\}$. A projection head f_p is applied to r_i^l to get the feature embedding z_i^l . For simplicity, we analyze the case with only two views, although the following analysis also applies to cases with more than two views.

The SSL objective consists of two components: alignment and constraint. The alignment component aims to maximize the similarity between the feature embeddings of the two views that share the same ancestor sample. The constraint component introduces additional prior knowledge to the learning process, such as the distribution of the embedding space and the parameter update rules. Consequently, SSL methods can be unified under a common framework, as expressed below:

$$\min_{f, f_p} \mathcal{L}_{\text{align}}(X_{tr}^{aug}, f, f_p) + \mathcal{L}_{\text{constrain}}(X_{tr}^{aug}, f, f_p), \quad (1)$$

where $\mathcal{L}_{\text{align}}$ and $\mathcal{L}_{\text{constrain}}$ denote the objectives of the alignment and constraint losses, which we detail in the following analysis.

SimCLR [1] randomly selects an anchor sample x_i^l from the augmented training set X_{tr}^{aug} . The sample x_i^{3-l} is considered

as the positive sample related to x_i^l for they share the same ancestor x_i . The remaining samples $X^- = X_{tr}^{aug} \setminus \{x_i^l, x_i^{3-l}\}$ are considered as the negative samples related to x_i^l .

The objective of SimCLR is defined as follows:

$$\mathcal{L}_{\text{NCE}} = \sum_{x_i^l \in X_{tr}^{aug}} -\log \frac{\exp(\text{sim}(x_i^l, x_i^{3-l})/\tau)}{\sum_{x_j^k \in X^- \cup \{x_i^{3-l}\}} \exp(\text{sim}(x_i^l, x_j^k)/\tau)}, \quad (2)$$

where τ is the temperature hyperparameter. Denote $z_i^l = f_p(f(x_i^l))$ as the projected feature embedding after the projection head f_p and feature extractor f , the similarity function $\text{sim}(x_i^l, x_i^{3-l}) = z_i^{lT} z_i^{3-l} / \|z_i^l\|_2 \|z_i^{3-l}\|_2$ calculates the cosine similarity between projected feature embedding of samples. According to [26], Equation 2 can be understood as aligning the embedding of x_i^l and x_i^{3-l} while constraining the feature embedding of all samples in $x_j^k \in X_{tr}^{aug}$ to satisfy a uniform distribution.

The main idea of BYOL [2] is to only increase the similarity between pairs of samples in X_{tr}^{aug} that share the same ancestor, without explicitly considering negative samples. BYOL considers two networks: the online network and the target network. The two networks have the same feature extraction module f and projection head module f_p . However, the online network has one more regression module f_r than the target network. The objective of BYOL can be viewed as the mean squared error (MSE) between the outputs of the online network and the target network, which can be presented as:

$$\mathcal{L}_{\text{BYOL}} = \sum_{i=1}^N \sum_{l=1}^2 \|f_r(\bar{z}_i^l) - \bar{z}_i^{3-l}\|^2 \quad (3)$$

where $z_i^l = f_p(f(x_i^l))$ and $\bar{z}_i^l = z_i^l / \|z_i^l\|_2$. Note that a stop-gradient technique is applied to the target network in the gradient back-propagation stage. For the sake of simplicity, we denote the target network as f_{target} , and the part of the online network that is similar in structure to f_{target} is denoted as f_{online} . Then, f_{target} is updated with a moving average of the parameters of the online network, which can be denoted as:

$$f_{\text{target}} \leftarrow \pi f_{\text{target}} + (1 - \pi) f_{\text{online}} \quad (4)$$

where $\pi \in [0, 1]$ represents a target decay rate. Equation 3 can be considered as aligning the feature embedding of different views while Equation 4 constrains the update rule through stop-gradient and moving average of parameters.

Barlow Twins [3] is an augmentation-based method that does not depend on a large number of negative samples and does not require a stop-gradient technique or asymmetric networks. It first computes the cross-correlation matrix C within a minibatch between $\{x_i^1\}_{i=1}^N$ and $\{x_i^2\}_{i=1}^N$ in the feature space. Then, we have:

$$C_{kj} = \frac{\sum_{i=1}^N z_{i,k}^1 \cdot z_{i,j}^2}{\sqrt{\sum_{i=1}^N (z_{i,k}^1)^2} \cdot \sqrt{\sum_{i=1}^N (z_{i,j}^2)^2}} \quad (5)$$

where $z_i^l = f_p(f(x_i^l))$, $k, j \in \{1, \dots, D\}$, and D is the dimension of z_i^l . Then, the objective of Barlow Twins is presented as follows:

$$\mathcal{L}_{\text{BT}} = \sum_{k=1}^D (1 - C_{kk})^2 + \lambda \sum_{k=1}^D \sum_{j=1, j \neq k}^D C_{kj}^2 \quad (6)$$

where λ is a positive constant trading of the importance of the first and second terms of the objective. Minimizing the first term of Equation 6 aligns the embedding of two views of x_i while minimizing the second term of Equation 6 constrains different vector components of these feature embeddings to be decorrelated.

MAE [8] first reshapes the ancestor sample into m patches, denoted as $x_i \in \mathbb{R}^{m \times s}$, where s represents the patch size (e.g., 16×16 for an image sample). A random binary mask $m \in 0, 1^m$ is applied to the sample x_i to generate two views of x_i , where $x_i^1 = x_i[m]$ and $x_i^2 = x_i[1 - m]$. The MAE model includes an encoder f and a decoder g . The encoder f takes one view, x_i^1 , as input and generates the feature representation z_i^1 . The decoder g then takes z_i^1 and the masked index m as input and attempts to reconstruct the other view, x_i^2 . The objective of MAE can be described with the following mean squared error loss:

$$\mathcal{L}_{\text{MAE}} = \sum_{i=1}^N \sum_{l=1}^2 \|g(f(x_i^l)) - x_i^{3-l}\|_2^2. \quad (7)$$

The above objective can also be applied to other reconstruction-based methods such as BEiT [16], SimMIM [9], and iBOT [27]. It is noteworthy that if we treat the masking strategy in reconstruction-based methods as an augmentation technique, Equation 7 can be considered as implicitly aligning the feature representation of x_i^l and x_i^{3-l} as suggested in [28]. Unlike augmentation-based methods, MAE enforces no explicit constraints, and this results in a dimensional collapse problem as suggested in [28].

IV. MOTIVATING EXAMPLE AND ANALYSIS

In this section, we first describe the crowding problem with experimental observation. Then, we propose an empirical analysis to understand why SSL methods suffer from this problem and derive a way to solve this problem: minimizing the intra-class variance and maximizing the inter-class separation while performing SSL. Finally, we show through theoretical analysis that only by minimizing the SSL loss, intra-class variance, and inter-class separability at the same time can we better reduce the upper bound of cross-entropy loss.

A. Motivating example

To provide a clear comparison between SSL methods and supervised learning, we conducted a series of experiments. First, we trained feature extractors using different SSL methods: SimCLR, BYOL, Barlow Twins, SwAV, and MAE. Additionally, we trained a feature extractor using supervised cross-entropy loss. All feature extractors except MAE are implemented as the ResNet-50 [29], while MAE uses ViT-B/16 [30]. They are pre-trained on the ImageNet dataset for 1000 epochs. Next, we evaluated the classification accuracies on the ImageNet validation set following the standard protocol by training a linear classifier on top of the feature extractor with the parameters of the feature extractor frozen. The accuracies are presented in Table I.

We observed that the accuracies for SSL are comparable but significantly lower than the accuracy of the supervised

method. Specifically, MAE has a significantly lower linear-eval accuracy, which is also observed by a series of works. To further analyze the learned encoders, we employed t-SNE [31] to visualize the data distribution of the ImageNet test data. The visualization results are depicted in Figure 1.

In Figure 1, each point represents an individual sample embedding, with different colors representing different categories.

We observe that embeddings with the same label cluster tightly together, while those with different labels are clearly separated by distinct borders. This indicates that the supervised method achieves a small intra-class variance and a large inter-class distance. Conversely, the embeddings produced by SSL methods, shown in Figures 1(a) to 1(e), do not exhibit clear separation, and the intra-class variance is large. We refer to this phenomenon as *the crowding problem*. Specifically, the cluster-based method SwAV (Figure 1(d)) demonstrates smaller intra-class variance, but the embeddings from different classes still overlap. The reconstruction-based method MAE (Figure 1(e)) shows very large intra-class variance, with embeddings from different classes failing to form distinct clusters. This corresponds to the poor linear evaluation performance seen in Table I. Other SSL methods, depicted in Figures 1(a), 1(c), and 1(b), exhibit some clustering characteristics, but with relatively large intra-class variance and overlapping class borders.

We provide a quantified analysis of the intra-class variance and inter-class distance for both SSL methods and the supervised method in Table I. In this table, the inter-class distance is calculated as the mean ℓ_2 -normalized Euclidean distance between embeddings of each class. The mean intra-class variance is calculated as the variance of the distances within embeddings of each class. Formally, for a test set $D_{te} = \{(x_i, y_i)\}_{i=1}^N$ with N pairs of samples x and labels y , the feature embedding of sample x is obtained using the feature extractor f as $z = f(x)$. The feature embedding is then ℓ_2 -normalized as $\bar{z} = z/\|z\|_2$. The mean embedding vector μ_i of class $i \in \{1, \dots, K\}$ is calculated with $\mu_i = \frac{1}{N_i} \sum_{j=1}^{N_i} \bar{z}_{i,j}$, where N_i is the number of samples in the i -th class. The inter-class distance is calculated as: $d_{\text{inter}} = \frac{2}{K(K-1)} \sum_{i=1}^{K-1} \sum_{j=i+1}^K \|\mu_i - \mu_j\|_2$. The intra-class variance of class i is calculated as: $\text{Var}_i = \frac{1}{N_i} \sum_{j=1}^{N_i} \|z_{i,j} - \mu_i\|_2^2$. The mean intra-class variance is the average intra-class variance over all classes, calculated as: $\text{Var}_{\text{intra}} = \frac{1}{K} \sum_{i=1}^K \text{Var}_i$. As

TABLE I
THE INTER-CLASS DISTANCE, THE INTRA-CLASS VARIANCE, AND THE LINEAR EVALUATION ACCURACY OF SSL METHODS.

Method	Inter-class Dist. (\uparrow)	Intra-class Var. (\downarrow)	ACC (%)
SimCLR	1.17	1.15	70.15
BYOL	0.90	0.65	71.48
SwAV	1.12	1.01	75.78
Barlow Twins	1.06	1.11	73.97
MAE	0.14	0.85	66.85
Supervised	1.32	0.62	79.24

shown in Table I, the MAE has the smallest inter-class distance and shows no clustering characteristic in Figure 1(e), this corresponds to the poor performance in linear-eval ACC. In contrast, the supervised method exhibits the smallest intra-class variance and the largest inter-class distance and also has a good

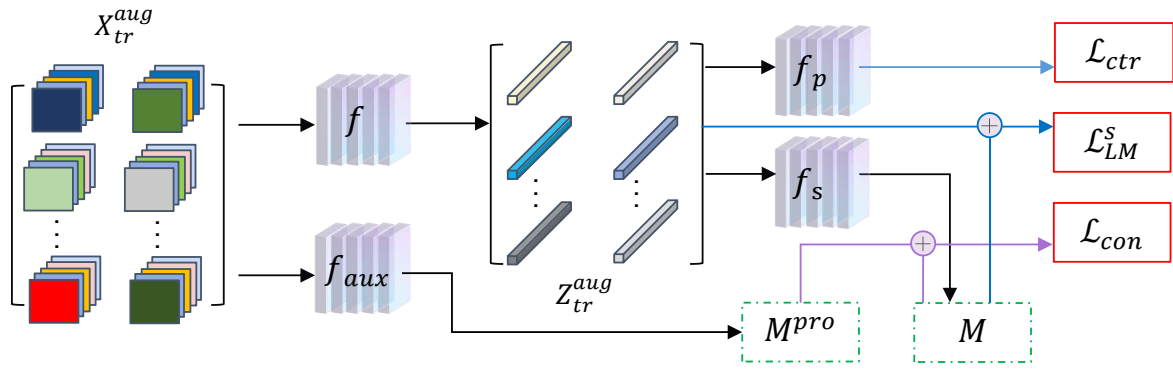


Fig. 2. The pipeline of the proposed DSA. First, DSA obtains the feature representations by the f_p and the M^{pro} by the f_p . Then, DSA obtains the M by the f_s . Finally, DSA simultaneously minimizes the \mathcal{L}_{ctr} , \mathcal{L}_{LM}^s , and \mathcal{L}_{con} to learn the model.

performance in linear-eval ACC. Other SSL methods either have smaller inter-class distances or larger intra-class variances, leading to sub-optimal linear-eval ACC performance. These quantified results underscore a significant connection between the crowding problem and downstream performance, aligning with the observed visualization patterns. Following this, we provide an empirical analysis of the SSL objectives introduced in Section III.

B. Empirical analysis

To elucidate the reasons behind the crowding problem observed in self-supervised methods, it is essential to gain an understanding of the underlying mechanisms employed by the self-supervised approaches described in Section III.

According to [26], minimizing Equation 2 aims to encourage the learned representations of positive pairs to exhibit similarity, while also constraining all samples in the feature space to be uniformly distributed on a unit hypersphere. In the case of BYOL, minimizing Equation 3 focuses solely on promoting similarity between the learned representations of two samples with the same ancestor. Similarly, for Barlow-Twins, minimizing Equation 6 aims to ensure that the learned representations of positive samples are similar to the anchor, while also encouraging the different dimensions of the learned representations to be independent of each other. According to [28], minimizing Equation 7 only encourages the alignment of the representation of two samples with the same ancestor with no additional constraints. This could lead to a collapse problem, where the inter-class distance is significantly lower than that of augmentation-based methods.

As we can see, these methods primarily focus on minimizing the distance between x_i^l and x_j^k . None of the SSL methods are explicitly designed to constrain the relationship between x_i^l and x_j^k , where $i, j \in \{1, 2, \dots, N\}$, $i \neq j$, and $l, k \in \{1, 2\}$. In contrast, supervised learning leverages labeled data to explicitly enforce the aggregation of similar points and the separation of different types of points. Consequently, some pairs in X_{tr}^{aug} are grouped together, while others are intentionally pushed apart.

In order to enhance the performance of self-supervised learning methods, it is necessary to adopt a criterion that enables the clustering of similar points and the separation

of dissimilar points. This realization leads us to propose the following approach.

C. Theoretical Analysis

To illustrate why we should minimize the intra-class variance and maximize the inter-class separation while performing contrastive learning, we first give an assumption on the label consistency between pairs in X_{tr}^{aug} with the same ancestor.

Assumption IV.1. $\forall \{x_i^1, x_i^2\} \in X_{tr}^{aug}$, assume the labels are deterministic (one-hot) and consistent: $p(y | x_i^1) = p(y | x_i^2)$.

Then, we aim to bound the generalization gap between unsupervised and supervised learning risks based on the classification task, which trains a softmax classifier by minimizing the mean cross entropy loss, e.g., $\mathcal{L}_{CE}^\mu(f) = \mathbb{E}_{p(x,y)}[-\log \exp(f(x)^T \mu_y) / \sum_{i=1}^K \exp(f(x)^T \mu_i)]$, where $p(x, y)$ represents the joint distribution of the input sample and the corresponding label, K represents the number of the class, $\mu_i = \mathbb{E}_{p(x|y)}[f(x)]$ is the cluster center of the i -th class and can be seen as the weight w_i of the linear classifier g , and $p(x|y)$ is the conditional distribution. Then, we have:

Theorem IV.1. If Assumption IV.1 holds, then, for any $f \in \mathcal{F}$, $\mathcal{L}_{CE}^\mu(f)$ can be bounded by $\mathcal{L}_{NCE}^\mu(f)$ as:

$$\mathcal{L}_{CE}^\mu(f) \leq \mathcal{L}_{NCE}^\mu(f) - const + \sum_{i=1, j=1, i \neq j}^K \mu_i^T \mu_j + \sqrt{\text{Var}(f(x)|y)} + O(const^{-1/2}) \quad (8)$$

where $const$ is a constant that is related to the number of negative samples, $\mu_i = \mathbb{E}_{p(x|i)}[f(x)]$, and $\text{Var}(f(x)|y) = \mathbb{E}_{p(y)}[\mathbb{E}_{p(x|y)}\|f(x) - \mathbb{E}_{p(x|y)}f(x)\|^2]$.

The detailed proof is illustrated in Appendix A. From empirical analysis and theoretical analysis, we can obtain that only by minimizing the contrastive loss, intra-class variance, and inter-class difference at the same time, can we reduce the upper bound of cross-entropy loss, thus, can we compress the upper bound of classification error. The empirical analysis and the theoretical analysis provide us with insights to design a new contrastive learning objective function, that is, to design an objective function that can measure intra-class variance and inter-class difference in an unsupervised way. In this paper, We

propose DSA to aggregate similar points together and separate different points from each other. Therefore, the proposed DSA is beneficial to compress the upper bound of $\mathcal{L}_{CE}^\mu(f)$.

V. METHODOLOGY

In this section, we describe our proposed method called Dynamic Semantic Adjuster (DSA). DSA can be easily integrated into existing self-supervised learning methods. The core concept of DSA is to attract samples with similar semantics while repelling others in an instance-based manner. Specifically, DSA first randomly selects a point from the training dataset as an anchor point, and then based on the arranging module and the scoring module, aggregates the points in the training dataset that are similar to the anchor point and separates the points that are dissimilar to the anchor point. Then DSA traverses all the points in the training dataset and treats them as anchor points, thus achieving the purpose of aggregating similar points and separating dissimilar points in the entire training dataset. Note that similar points are more likely to be of the same class, and dissimilar points are more likely to be of different classes. Therefore, DSA can induce a clustering structure and make points of the same class cluster together, thereby reducing intra-class variance, and make points of different classes separate from each other, thereby enhancing inter-class separation.

The overall pipeline of DSA is illustrated in Figure 2, it consists of two main components. The first component is the arranging module, which groups samples with similar semantics together and pushes away those with dissimilar semantics. The second component is the scoring module, which is to further revise the semantic similarity between samples in the arranging module through the relative position structure between samples in the original space.

A. Arranging module

The arranging module (AM) is designed to learn a regulator M , which guides the arrangement of samples in the feature space. The goal of the regulator M is to bring samples with high similarity closer to each other while separating samples with low similarity. Formally, the regulator M can be interpreted as a similarity matrix with a size of $2N \times 2N$.

Specifically, we first project each sample in $X_{tr}^{aug} = \{x_1^1, x_1^2, \dots, x_N^1, x_N^2\}$ to the feature space via f and obtain their feature representations, denoted as $Z_{tr}^{aug} = \{z_1^1, z_1^2, \dots, z_N^1, z_N^2\}$, where $z_i^l = f(x_i^l)$, $i \in \{1, \dots, N\}$, and $l \in \{1, 2\}$. Regarding the i -th sample z_i in Z_{tr}^{aug} as the anchor, then, for the j -th sample z_j in Z_{tr}^{aug} , we concatenate them and obtain a new representation $z_{i,j}$, e.g., $z_{i,j} = \text{cat}(z_i, z_j)$. Subsequently, we feed $z_{i,j}$ into a similarity network f_s , which consists of a two-layer MLP with ReLU activation function. The selection of f_s is evaluated and discussed through an ablation study in Section VI-F. The similarity network computes the similarity value between z_i and z_j and assigns it to the corresponding entry $M_{i,j}$ in the regulator matrix M , i.e., $M_{i,j} = f_s(z_{i,j})$. Then, based on the anchor z_i , we can obtain:

$$M_i = [\bar{f}_s(z_{i,1}), \dots, \bar{f}_s(z_{i,2N})] \quad (9)$$

where $\bar{f}_s(z_{i,j}) = f_s(z_{i,j}) / \sum_{k=1}^{2N} f_s(z_{i,k})$ and $j \in \{1, \dots, 2N\}$. We in turn treat the samples in Z_{tr}^{aug} as anchors and obtain $M = [M_1, \dots, M_{2N}]^T$.

Once the regulator matrix M is obtained, we propose to minimize the following loss function:

$$\mathcal{L}_{AM} = \log\left(1 + \sum_{i=1}^{2N} \sum_{j=1}^{2N} \exp\left(\frac{(2M_{i,j} - \alpha) \|z_i - z_j\|_2^2}{\tau}\right)\right) \quad (10)$$

where $\tau, \alpha > 0$ are two temperature hyperparameters. Note that \mathcal{L}_{AM} captures not only the relationship between different augmentations of the same ancestor but also the relationship between different augmentations of different ancestors.

Given α and $M_{i,j}$, when $2M_{i,j} - \alpha > 0$, we consider that the samples z_i and z_j in Z_{tr}^{aug} are semantically similar and should be brought closer together. From Equation (10), we can obtain that when $2M_{i,j} - \alpha > 0$, minimizing $\|z_i - z_j\|_2^2$ can minimize \mathcal{L}_{AM} . Also, to minimize \mathcal{L}_{AM} , the greater the value of $2M_{i,j} - \alpha$, the closer we should pull z_i and z_j . Therefore, we can conclude that minimizing \mathcal{L}_{AM} can bring different pairs closer to different degrees according to the value of $M_{i,j}$.

B. Scoring module

As illustrated in the above subsection, $M_{i,j}$ can control the dynamics (move closer to or farther away from the anchor) of a sample. However, M is obtained by inputting $z_{i,j}$ into f_s . Without proper constraints, f_s may output undesirable values. For example, in the initial stage of training, the performance of f_s is often poor, which leads to the learned regulator matrix being inaccurate, causing the sample points in the training dataset to be incorrectly aggregated and separated. To alleviate this problem, we propose a scoring module (SM) that can revise the output of f_s based on the similarity prior of the samples in the original input space.

Specifically, we first input samples in X_{tr}^{aug} into an auxiliary feature extractor f_{aux} to obtain prior feature representations, denoted as $\bar{Z}_{tr}^{aug} = \{\bar{z}_1^1, \bar{z}_1^2, \dots, \bar{z}_{2N}^1, \bar{z}_{2N}^2\}$, where $\bar{z}_i^l = f_{aux}(x_i^l)$, $i \in \{1, \dots, 2N\}$, and $l \in \{1, 2\}$. Then, considering the i -th element \bar{z}_i in \bar{Z}_{tr}^{aug} as the anchor, we define:

$$M_{i,j}^{pro} = \exp\left(\frac{\|\bar{z}_i - \bar{z}_j\|_2^2}{\tau}\right) \quad (11)$$

where \bar{z}_j is the j -th sample in \bar{Z}_{tr}^{aug} . Then, we can obtain:

$$M_i^{pro} = [\bar{M}_{i,1}^{pro}, \dots, \bar{M}_{i,2N}^{pro}] \quad (12)$$

where $\bar{M}_{i,k}^{pro} = M_{i,k}^{pro} / \sum_{j=1}^{2N} M_{i,j}^{pro}$ and $k \in \{1, \dots, 2N\}$. We in turn treat the samples in \bar{z}_i as anchors and obtain $M^{pro} = [M_1^{pro}, \dots, M_{2N}^{pro}]^T$. To this end, we give the prior constraint M^{pro} of M based on the Euclidean distance of different pairs of samples in the original input space. We constrain M as follows:

$$\mathcal{L}_{con} = \|M^{pro} - M\|_2^2 \quad (13)$$

By simultaneously minimizing Equation (13) and Equation (10), the points in the original input space that are closer to the anchor become attracted to a closer location in the learned feature space, while the points that are farther from the anchor are repelled to a more distant location in the feature space.

To assess the quality of each anchor, we propose a scoring mechanism based on the connectivity between samples. Given the i -th element z_i in Z_{tr}^{aug} , we find its corresponding element \bar{z}_i in \bar{Z}_{tr}^{aug} . We then identify the η nearest neighbors of it in \bar{Z}_{tr}^{aug} based on Euclidean distance and denote them as $N_\eta(\bar{z}_i)$. The connection score s_i for anchor z_i is defined as:

$$s_i(z_i) = \sum_{\bar{z}_i^b \sim N_\eta(\bar{z}_i^a), \bar{z}_i^a \sim N_\eta(\bar{z}_i)} \mathbb{1}_{\{\bar{z}_i \in N_\eta(\bar{z}_i^b)\}} \quad (14)$$

Then, we score the quality of z_i as:

$$sc(z_i) = s_i(z_i)/\eta \quad (15)$$

The scoring mechanism in Equation (14) takes into account both direct connections between the anchor \bar{z}_i and $N_\eta(\bar{z}_i)$ as well as latent connections induced by other samples along the connected path [32]. From Equation (15), we can deduce that when z_i is surrounded by points of the same class, $s_i(z_i)$ should be equal to or slightly smaller than η . Consequently, the score $sc(z_i)$ is equal to or slightly smaller than 1, and when z_i is an outlier, $s_i(z_i)$ should be close to 0, which is much smaller than η , so that $sc(z_i)$ is also close to 0. Therefore, to reduce the influence of bad anchors, we weight Equation (10) and obtain the following:

$$\mathcal{L}_{AM}^s = \log\left(1 + \sum_{i=1}^{2N} (sc(z_i) \cdot \sum_{j=1}^{2N} \exp\left(\frac{(2M_{i,j}-\alpha)\|z_i-z_j\|_2^2}{\tau}\right))\right) \quad (16)$$

C. Overall objective

To this end, the objective of the proposed DSA is shown as:

$$\mathcal{L}_{DSA}^s = \mathcal{L}_{ssl} + \nu \mathcal{L}_{AM}^s + v \mathcal{L}_{con} \quad (17)$$

where \mathcal{L}_{ssl} is the loss of contrastive learning, e.g., we can set \mathcal{L}_{ssl} equals to \mathcal{L}_{NCE} , \mathcal{L}_{BYOL} , \mathcal{L}_{BT} , or \mathcal{L}_{MAE} , and $\nu, v > 0$ represent the temperature hyperparameters.

First, minimizing the second term of equation (17) can aggregate similar samples and separate dissimilar samples according to the similarity of sample points. Second, minimizing the second term of the equation (17) can eliminate the outliers in the training samples, so that the process of aggregating and separating samples is not affected by outliers. Minimizing the third term of equation (17) can make the similarity between samples obtained by a more accurate, thereby making a better at aggregating and separating samples. Combined with Theorem IV.1, minimizing the second and third terms of the equation (17) at the same time can not only reduce intra-class variance but also improve inter-class separability, thus, can compress the upper bound of classification error.

VI. EXPERIMENT

In this section, we assess the performance of our proposed DSA through extensive experiments. First, we briefly introduced the benchmark datasets for evaluation. Then, we detail the implementation of the DSA pre-training process, and we evaluate its performance on standard benchmarks for self-supervised image and video representation learning. To demonstrate the superior generalization capabilities of our method, we also apply DSA to various downstream

tasks, including semi-supervised classification, object detection, few-shot learning and semantic segmentation. Finally, we present a comprehensive ablation study on hyper-parameters, module design, and complexity, along with case studies for visualization.

A. Benchmark dataset

Our experiments involved various datasets across different tasks. The pre-training dataset for image data is ImageNet[11], which contains 1.3 million training images across 1000 classes. The pre-training dataset for video data is the Kinetics 400 dataset [33], which contains 400 human action classes, with at least 400 video clips for each action. Each clip lasts around 10s and is taken from different YouTube videos. The downstream object detection and instance segmentation for image data are evaluated on the MS-COCO [34] and Pascal-VOC [35] dataset. MS-COCO is a large-scale object detection, segmentation, key-point detection, and captioning dataset consisting of 328K images. The Pascal-VOC dataset includes 1464 training images and 1449 validation images, annotated with object segmentation, bounding boxes, and class labels. It covers 20 different object categories.

The few-shot classification is evaluated on few-shot learning benchmarks: FC100 [36], Caltech-UCSD Birds (CUB-200) [37], and Plant Disease [38]. FC-100 is a split dataset based on CIFAR-100[39] and designed for few-shot learning by split training, validation, and testing classes to minimize the information overlap between splits. CUB-200 consists of 6033 bird images classified into 200 bird species. Plant Disease is a public dataset containing 54306 images of diseased and healthy plant leaves, the label contains 14 crop species and 26 diseases.

B. Pre-training Details

The SSL pre-training for image data follows the standard protocol using the Lightly-SSL framework [40] on the ImageNet [11] dataset. The pre-training epoch on ImageNet is 1000 epochs. We use a learning rate warm-up for the first 500 iterations of the optimizer and a 0.2 learning rate drop at 50 and 25 epochs before the end. Our proposed method is integrated with benchmark SSL algorithms with either ResNet-50 or ViT-B as the backbone network. The SSL pre-training for video data follows the standard protocol as introduced in [41] on the Kinetics 400 dataset [33]. The pre-training backbone networks include R3D-18, R3D-50, and ViT-B. We integrate our method with four well-known video SSL algorithms: v-MoCo, v-BYOL, v-SimCLR, and v-SwAV. We evaluate the video SSL algorithm on two backbones, R3D-18[42] and R3D-50[43]. The default training epoch is 200 while the default batch size is 256. For the default hyperparameters of DSA, we set the number of neighbors $\eta = 20$, the hyperparameter $\alpha = 1.0$, $\nu = 0.1$, and $v = 100$. We conduct a detailed ablation study of these hyper-parameters in Section VI-F.

C. Standard Evaluation

To evaluate the performance of the pre-trained feature extractor with our proposed method, we perform the standard

TABLE II

THE TOP-1 AND TOP-5 CLASSIFICATION ACCURACIES OF A LINEAR CLASSIFIER ON IMAGENET WITH RESNET-50 AS THE FEATURE EXTRACTOR.

Method	Backbone	Top-1	Top-5
SimCLR [1]	ResNet-50	70.15 ± 0.16	89.75 ± 0.14
MoCo [44]	ResNet-50	72.80 ± 0.12	91.64 ± 0.11
BYOL [2]	ResNet-50	71.48 ± 0.15	92.32 ± 0.14
SimSiam [13]	ResNet-50	73.01 ± 0.21	92.61 ± 0.27
Barlow Twins [3]	ResNet-50	73.97 ± 0.23	92.91 ± 0.19
SwAV [10]	ResNet-50	75.78 ± 0.16	92.86 ± 0.15
DINO [6]	ResNet-50	75.43 ± 0.18	93.32 ± 0.19
W-MSE [14]	ResNet-50	76.01 ± 0.27	93.12 ± 0.21
RELIC v2 [45]	ResNet-50	75.88 ± 0.15	93.52 ± 0.13
LMCL [46]	ResNet-50	75.89 ± 0.19	92.89 ± 0.28
ReSSL [47]	ResNet-50	75.77 ± 0.21	92.91 ± 0.27
SSL-HSIC [48]	ResNet-50	74.99 ± 0.19	93.01 ± 0.20
CorInfoMax [49]	ResNet-50	75.54 ± 0.20	92.23 ± 0.25
MEC [50]	ResNet-50	75.38 ± 0.17	92.84 ± 0.20
VICRegL [51]	ResNet-50	75.96 ± 0.19	92.97 ± 0.26
SimCLR + DSA	ResNet-50	72.09 ± 0.16	91.39 ± 0.13
MoCo + DSA	ResNet-50	74.79 ± 0.69	93.65 ± 0.74
SimSiam + DSA	ResNet-50	74.09 ± 0.89	94.24 ± 0.82
Barlow Twins + DSA	ResNet-50	76.03 ± 0.49	93.95 ± 0.15
SwAV + DSA	ResNet-50	77.84 ± 0.32	94.05 ± 0.89
DINO + DSA	ResNet-50	76.50 ± 0.78	94.46 ± 0.62
BYOL + DSA	ResNet-50	74.95 ± 0.57	94.93 ± 0.16
ReSSL + DSA	ResNet-50	77.45 ± 0.33	94.23 ± 0.23
VICRegL + DSA	ResNet-50	78.15 ± 0.63	94.04 ± 0.20
MAE [8]	ViT-B	66.85 ± 0.23	85.24 ± 0.43
U-MAE [28]	ViT-B	70.46 ± 0.18	91.25 ± 0.28
MoCo-v3 [52]	ViT-B	76.47 ± 0.14	93.76 ± 0.46
DINO [6]	ViT-B	78.17 ± 0.57	96.14 ± 0.17
MAE + DSA [8]	ViT-B	72.76 ± 0.41	89.36 ± 0.31
MoCo-v3 + DSA [52]	ViT-B	78.24 ± 0.72	95.75 ± 0.23
DINO + DSA [6]	ViT-B	79.20 ± 0.42	97.16 ± 0.66

TABLE III

LINEAR EVALUATION RESULTS ON THE KINETICS-400 DATASET, WHERE ϱ , L , AND δ DENOTE THE NUMBER OF POSITIVE SAMPLES, CLIP LENGTH, AND STRIDE, RESPECTIVELY.

Method	ϱ	L	δ	Top-1
supervised	-	8	8	74.7
v-SimCLR [41]	2	8	8	60.5
v-BYOL [41]	2	8	8	65.8
v-MoCo [41]	2	8	8	65.8
v-SwAV [41]	2	8	8	61.6
v-SimCLR + DSA	2	8	8	62.5
v-BYOL + DSA	2	8	8	66.7
v-MoCo + DSA	2	8	8	67.3
v-SwAV + DSA	2	8	8	62.8

evaluation protocol, i.e. linear evaluation on the obtained feature extractors. This protocol involves freezing the feature extractor $f(\cdot)$ after pre-training and subsequently training a supervised linear classifier with softmax on top of it. We present the average top-1 and top-5 accuracy and the standard deviation of 5 runs for pre-trained image feature extractor in Table II. While the linear evaluation results for video data is shown in Table III.

From Table II, we can observe that the inclusion of DSA significantly improves the linear evaluation performance compared to the SSL baselines, with an increase in average top-1 accuracy by 2.04%, and an increase in top-5 accuracy by 1.57%. Furthermore, DSA is effective across different

TABLE IV

THE SEMI-SUPERVISED LEARNING ACCURACIES (%) ON IMAGENET USING 1% AND 10% TRAINING EXAMPLES. DATASET WITH THE RESNET-50 PRE-TRAINED ON THE IMAGENET DATASET.

Method	1%		10%	
	Top-1	Top-5	Top-1	Top-5
Supervised	25.1 ± 1.3	48.6 ± 0.7	55.9 ± 0.7	81.2 ± 0.8
SimCLR [1]	48.3 ± 0.2	75.5 ± 0.1	65.6 ± 0.1	87.8 ± 0.2
MoCo [44]	52.3 ± 0.1	77.9 ± 0.2	68.4 ± 0.1	88.0 ± 0.2
BYOL [2]	56.3 ± 0.2	79.6 ± 0.2	69.7 ± 0.2	89.3 ± 0.1
SimSiam [13]	54.9 ± 0.2	79.5 ± 0.2	68.0 ± 0.1	89.0 ± 0.3
Barlow Twins [3]	55.0 ± 0.1	79.2 ± 0.1	67.7 ± 0.2	89.3 ± 0.2
RELIC v2 [45]	55.2 ± 0.2	80.0 ± 0.1	68.0 ± 0.2	88.9 ± 0.2
LMCL [46]	54.8 ± 0.2	79.4 ± 0.2	70.3 ± 0.1	89.9 ± 0.2
ReSSL [47]	55.0 ± 0.1	79.6 ± 0.3	69.9 ± 0.1	89.7 ± 0.1
SSL-HSIC [48]	55.1 ± 0.3	79.6 ± 0.2	70.4 ± 0.1	90.0 ± 0.1
CorInfoMax [49]	55.0 ± 0.2	79.6 ± 0.3	70.3 ± 0.2	89.3 ± 0.2
MEC [50]	54.8 ± 0.1	79.4 ± 0.2	70.0 ± 0.1	89.1 ± 0.1
VICRegL [51]	54.9 ± 0.1	79.6 ± 0.2	67.2 ± 0.1	89.4 ± 0.2
SimCLR + DSA	49.9 ± 0.2	77.3 ± 0.1	66.6 ± 0.1	89.3 ± 0.2
MoCo + DSA	54.1 ± 0.3	80.0 ± 0.3	69.9 ± 0.3	90.0 ± 0.2
BYOL + DSA	57.5 ± 0.5	81.1 ± 0.1	71.7 ± 0.4	91.0 ± 0.3
Barlow Twins + DSA	57.0 ± 0.1	80.9 ± 0.1	69.4 ± 0.5	90.7 ± 0.1

backbones, with an average improvement of top-1 accuracy of 1.88% for ViT-B and 2.13% for ResNet-50. Also, when using ResNet-50 as the backbone, VICRegL+DSA achieved the highest average top-1 accuracy of 78.15%, surpassing the best previous result of W-MSE by 2.14%, when using ViT-B as the backbone, DINO+DSA achieved the highest average top-1 accuracy of 79.20%, exceeding that of DINO by 1.05%. Moreover, despite the linear evaluation results of MAE being significantly lower compared to other methods, the introduction of DSA results in a notable improvement, with an increase in top-1 accuracy by 5.91%.

From Table III, we can observe that the addition of DSA leads to an average increase of 1.4% in the top-1 accuracy of action classification by SSL algorithms on the Kinetics-400 validation set. This demonstrates that our proposed DSA is not only applicable to a specific type of data but is effective across various data modalities.

In summary, DSA significantly enhances the accuracy of SSL methods on the validation set during standard linear evaluation, aligning with the conclusions drawn from our theoretical analysis.

D. Downstream Evaluation

To further explore the performance of our proposed DSA, we tested the pre-trained SSL feature extractor on a range of downstream tasks. These tasks include semi-supervised classification, action recognition, few-shot classification, object detection, instance segmentation, and action detection. Experimental results indicate that DSA achieves significant improvements across all these downstream tasks.

a) *Semi-Supervised Classification*: We follow the setting of [1] and sample 1% and 10% of the labeled data from ImageNet [11] in a class-balanced way, with each class containing around 12.8 to 128 images per class respectively. We then fine-tune the pre-trained backbone with our method for 50 epochs with these sampled labeled data and report the average top-1 and top-5 accuracies of the test set.

TABLE V
FINETUNING RESULTS (AVERAGE OF 3 SPLITS) FOR ACTION CLASSIFICATION ON UCF101 AND HMDB51. SELF-SUPERVISED PRE-TRAINING IS DONE ON KINETICS 400 DATASETS. ϱ IS THE NUMBER OF POSITIVE SAMPLES.

Method	Resolution	Frames	Architecture	Param.	Epochs	UCF101	HMDB51
VTHCL [53]	224×224	8	R3D-18	13.5M	200	80.6	48.6
TCLR [54]	112×112	16	R3D-18	13.5M	100	85.4	55.4
VideoMoCo [55]	112×112	16	R3D-18	13.5M	200	74.1	43.6
SLIC [56]	128×128	32	R3D-18	13.5M	150	83.2	52.2
MACLR [57]	112×112	32	R3D-18	13.5M	600	91.3	62.1
v-BYOL $_{\varrho=4}$	112×112	16	R3D-18	13.5M	200	88.3	69.3
v-BYOL $_{\varrho=4}$ + DSA	112×112	16	R3D-18	13.5M	200	92.7	70.5
CVRL [58]	224×224	32	R3D-50	31.8M	800	92.2	66.7
MACLR [57]	224×224	32	R3D-50	31.8M	600	94.0	67.4
v-SimCLR $_{\varrho=2}$ [41]	224×224	8	R3D-50	31.8M	200	88.9	67.2
v-SwAV $_{\varrho=2}$ [41]	224×224	8	R3D-50	31.8M	200	87.3	68.3
v-MoCo $_{\varrho=4}$ [41]	224×224	8	R3D-50	31.8M	200	93.5	71.6
v-BYOL $_{\varrho=4}$ [41]	224×224	8	R3D-50	31.8M	200	94.2	72.1
v-SimCLR $_{\varrho=2}$ + DSA	224×224	8	R3D-50	31.8M	200	90.7	69.5
v-SwAV $_{\varrho=2}$ + DSA	224×224	8	R3D-50	31.8M	200	91.1	69.7
v-MoCo $_{\varrho=4}$ + DSA	224×224	8	R3D-50	31.8M	200	94.9	73.7
v-BYOL $_{\varrho=4}$ + DSA	224×224	8	R3D-50	31.8M	200	95.4	73.6

TABLE VI
FEW-SHOT LEARNING ACCURACIES (%) WITH 95% CONFIDENCE INTERVALS AVERAGED OVER 2000 EPISODES ON FC100, CUB200, AND PLANT DISEASE. (N, K) DENOTES N -WAY K -SHOT TASKS.

Method	FC100		CUB200		Plant Disease	
	(5,1)	(5,5)	(5,1)	(5,5)	(5,1)	(5,5)
Supervised	34.62 ± 0.88	47.15 ± 0.23	47.34 ± 0.66	64.87 ± 0.21	70.08 ± 0.24	89.83 ± 0.41
SimCLR [1]	39.89 ± 0.28	49.83 ± 0.70	44.47 ± 0.76	67.33 ± 0.65	76.94 ± 0.56	89.73 ± 0.67
Barlow Twins [3]	40.02 ± 0.73	52.69 ± 0.11	46.02 ± 0.21	65.06 ± 0.54	79.37 ± 0.11	89.53 ± 0.42
BYOL [3]	36.41 ± 0.43	51.36 ± 0.59	44.38 ± 0.33	62.75 ± 0.27	79.41 ± 0.24	91.05 ± 0.31
W-MSE [14]	40.97 ± 0.62	53.69 ± 0.56	49.15 ± 0.63	65.15 ± 0.74	75.52 ± 0.24	89.05 ± 0.64
VICRegL [51]	40.78 ± 0.48	54.28 ± 0.66	49.44 ± 0.82	67.18 ± 0.61	79.36 ± 0.22	92.84 ± 0.24
SimSiam [13]	37.11 ± 0.86	51.64 ± 0.32	46.28 ± 0.68	63.25 ± 0.14	76.83 ± 0.16	90.45 ± 0.75
ReSSL [47]	37.92 ± 0.64	52.35 ± 0.43	46.42 ± 0.42	63.76 ± 0.45	77.25 ± 0.86	91.15 ± 0.76
SwAV [10]	39.64 ± 0.11	51.83 ± 0.55	47.34 ± 0.16	65.24 ± 0.75	79.41 ± 0.35	92.62 ± 0.61
SimCLR + DSA	43.04 ± 0.37	52.38 ± 0.15	46.96 ± 0.12	70.52 ± 0.37	78.31 ± 0.71	91.23 ± 0.82
Barlow Twins + DSA	41.42 ± 0.88	55.47 ± 0.67	47.36 ± 0.39	68.04 ± 0.32	82.18 ± 0.73	90.95 ± 0.18
BYOL + DSA	39.85 ± 0.61	52.95 ± 0.46	46.13 ± 0.69	64.79 ± 0.76	82.89 ± 0.74	94.72 ± 0.89
SwAV + DSA	41.03 ± 0.21	54.12 ± 0.56	49.36 ± 0.10	68.27 ± 0.55	81.34 ± 0.68	93.20 ± 0.26

The results for semi-supervised classification are shown in Table IV. These results demonstrate that when the amount of labeled data is limited, the fine-tuning performance of pre-trained models based on self-supervised learning methods surpasses that of supervised baselines. Additionally, the pre-trained models incorporating the DSA method exhibit superior performance in semi-supervised tasks compared to their self-supervised baseline counterparts. With only 1% of labeled training data, the average top-1 accuracy increases by 1.65%, and the top-5 accuracy increases by 1.78%. With 10% of labeled training data, the average top-1 accuracy increases by 1.73%, and the top-5 accuracy increases by 1.73%.

Furthermore, compared to the best result with 1% labeled data, RELIC v2, BYOL+DSA exceeds its top-1 accuracy by 2.3% and its top-5 accuracy by 1.1%. Compared to the best result with 10% labeled data, SSL-HSIC, BYOL+DSA exceeds its top-1 accuracy by 1.3% and its top-5 accuracy by 1.0%.

In summary, the inclusion of DSA results in significant improvements in semi-supervised classification tasks. This indicates that enhancing model discriminability has a notable impact on the fine-tuning of downstream classification tasks, even when labeled data is limited.

b) Action Recognition: To evaluate the performance of the video pre-trained models, we follow the setting in [58], [41] and fine-tune them on UCF-101 and HMDB-51 datasets. We use the pre-trained backbone on Kinetics to initialize the network parameters and append additionally a classification layer. On each dataset, the models are trained for 50 epochs with a batch size of 128. The fine-tuning action recognition results are present in Table V. For a fair comparison with other video SSL baseline methods with small-scale feature extractors, we also report the fine-tuning results with R3D-18 [42] as the backbone. From the table, it can be seen that in the action recognition task, the accuracy with the addition of

TABLE VII

THE RESULTS OF TRANSFER LEARNING ON OBJECT DETECTION AND INSTANCE SEGMENTATION WITH C4-BACKBONE AS THE FEATURE EXTRACTOR. “AP” IS THE AVERAGE PRECISION, “AP_N” REPRESENTS THE AVERAGE PRECISION WHEN THE IOU (INTERSECTION AND UNION RATIO) THRESHOLD IS N%.

Method	VOC 07 detection			VOC 07+12 detection			COCO detection			COCO instance segmentation		
	AP ₅₀	AP	AP ₇₅	AP ₅₀	AP	AP ₇₅	AP ₅₀	AP	AP ₇₅	AP ₅₀ ^{mask}	AP ^{mask}	AP ₇₅ ^{mask}
Supervised	74.4	42.4	42.7	81.3	53.5	58.8	58.2	38.2	41.2	54.7	33.3	35.2
SimCLR [1]	75.9	46.8	50.1	81.8	55.5	61.4	57.7	37.9	40.9	54.6	33.3	35.3
MoCo [44]	77.1	46.8	52.5	82.5	57.4	64.0	58.9	39.3	42.5	55.8	34.4	36.5
BYOL [2]	77.1	47.0	49.9	81.4	55.3	61.1	57.8	37.9	40.9	54.3	33.2	35.0
SimSiam [13]	77.3	48.5	52.5	82.4	57.0	63.7	59.3	39.2	42.1	56.0	34.4	36.7
Barlow Twins [3]	75.7	47.2	50.3	82.6	56.8	63.4	59.0	39.2	42.5	56.0	34.3	36.5
SwAV [10]	75.5	46.5	49.6	82.6	56.1	62.7	58.6	38.4	41.3	55.2	33.8	35.9
MEC [50]	77.4	48.3	52.3	82.8	57.5	64.5	59.8	39.8	43.2	56.3	34.7	36.8
RELIC v2 [45]	76.9	48.0	52.0	82.1	57.3	63.9	58.4	39.3	42.3	56.0	34.6	36.3
CorInfoMax [49]	76.8	47.6	52.2	82.4	57.0	63.4	58.8	39.6	42.5	56.2	34.8	36.5
VICRegL [51]	75.9	47.4	52.3	82.6	56.4	62.9	59.2	39.8	42.1	56.5	35.1	36.8
SimCLR + DSA	77.5	47.9	52.0	83.6	57.5	63.9	59.0	39.5	42.9	56.3	35.4	36.3
MoCo + DSA	79.4	48.2	54.1	84.4	58.6	66.4	61.0	40.8	44.3	57.1	36.2	38.9
BYOL + DSA	78.5	48.4	52.1	83.1	57.0	62.6	59.0	39.3	43.3	55.8	35.3	37.2
SimSiam + DSA	78.7	50.1	54.2	84.7	58.3	65.0	60.4	41.0	43.2	58.1	36.9	38.9
SwAV + DSA	77.4	48.1	52.0	83.9	58.5	64.9	60.3	40.1	43.8	57.2	35.1	37.6
VICRegL + DSA	78.4	49.1	54.6	83.8	57.8	64.8	60.6	42.2	43.4	57.7	37.5	38.2

DSA shows an average improvement of 1.94% compared to the video self-supervised learning baseline. Additionally, when using R3D-18 as the backbone and only 16-frame video clips as input, v-BYOL + DSA exceeds the best-performing MACLR by 1.4% on the UCF-101 dataset.

These results demonstrate that the inclusion of DSA significantly enhances accuracy in downstream action recognition tasks for video SSL. This further indicates that our method improves the discriminability of the learned representations.

c) Few-shot Classification: We evaluate the few-shot classification on FC100, CUB200, and Plant Disease following the standard cross-domain few-shot setting [59], [60]. We evaluate the few-shot classification by performing logistic regression using the pre-trained ResNet-50 with the parameters frozen and report the results for both the 5-way 1-shot and 5-way 5-shots task in Table VI. From the results, we can observe that in few-shot classification tasks, SSL methods with DSA show an average accuracy improvement of 2.26% compared to their baselines. Moreover, the inclusion of DSA achieves better results across different datasets. For instance, in the 5-way 1-shot task on the FC100 dataset, the best self-supervised learning result is 40.97% achieved by W-MSE. In contrast, SimCLR + DSA exceeds this metric by 2.07%. Similarly, in the 5-way 5-shot task on the Plant Disease dataset, VICRegL achieves an average accuracy of 92.84%, while BYOL + DSA surpasses this result by 1.88%.

These findings indicate that the addition of DSA significantly enhances the performance of SSL in few-shot classification tasks.

d) Detection and Segmentation: The evaluation of downstream detection and segmentation tasks are evaluated on Pascal-VOC and MS-COCO datasets. For object detection on Pascal-VOC, we fine-tune a Faster R-CNN [61] with the C4-backbone. Results are reported for fine-tuning on the VOC 2007 trainval split and the combined VOC 2007 trainval + 2012 train split, both evaluated on the VOC 2007 test split. For object detection on COCO, we fine-tune a Mask R-CNN [62] (1× schedule)

with the C4-backbone. Fine-tuning is performed on the COCO 2017 train set and evaluated on the COCO 2017 val set.

The evaluation tasks on VOC and COCO follow the protocols outlined in [1], [3], [13], where the pre-trained Resnet-50 are used for initialization. We report the Average Precision (AP) at different intersections over union (IoU) ratios for results from VOC and COCO in Table VII.

TABLE VIII

THE INTER-CLASS DISTANCE, THE INTRA-CLASS VARIANCE, AND THE LINEAR EVALUATION ACCURACY OF SSL METHODS.

Method	Inter-class Dist. (↑)	Intra-class Var. (↓)
SimCLR	1.17	1.15
BYOL	0.9	0.65
SwAV	1.12	1.01
Barlow Twins	1.06	1.11
MAE	0.14	0.85
Supervised	1.32	0.62
SimCLR + DSA	1.37	0.92
BYOL + DSA	1.21	0.55
SwAV + DSA	1.31	0.57
Barlow Twins + DSA	1.15	0.97
MAE + DSA	0.64	0.65

From the results in Table VII, it can be seen that the inclusion of DSA significantly improves the AP in object detection and instance segmentation tasks. Specifically, in the VOC 07 detection task, the method with DSA shows an average AP improvement of 1.42% compared to the SSL baseline. In the VOC 07+12 detection task, the average AP increases by 2.11%. In the COCO detection task, the average AP increases by 1.65%, and in the COCO instance segmentation task, the average AP increases by 1.78%.

Based on the above results, it can be concluded that incorporating DSA in the self-supervised pre-training process can significantly enhance its effectiveness in downstream detection and instance segmentation tasks.

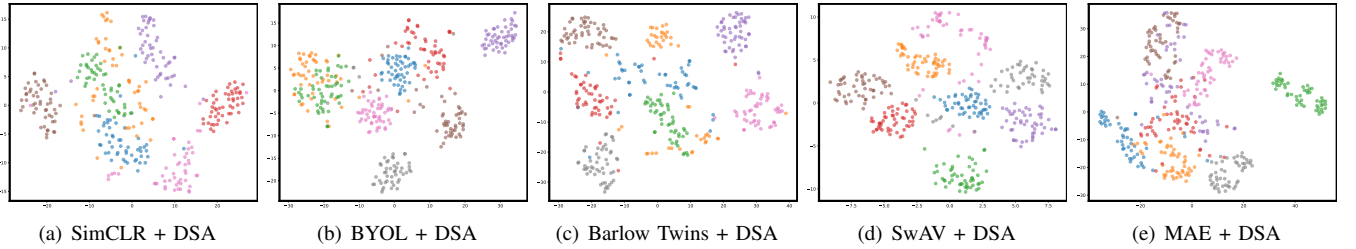


Fig. 3. Data distribution visualization based on 8 random classes of the test set of ImageNet in the feature space. (a) - (e) corresponds to the visualization results of the self-supervised methods integrated with DSA. We can observe that the border between classes is not overlapped, and the inter-class features are clustered together.

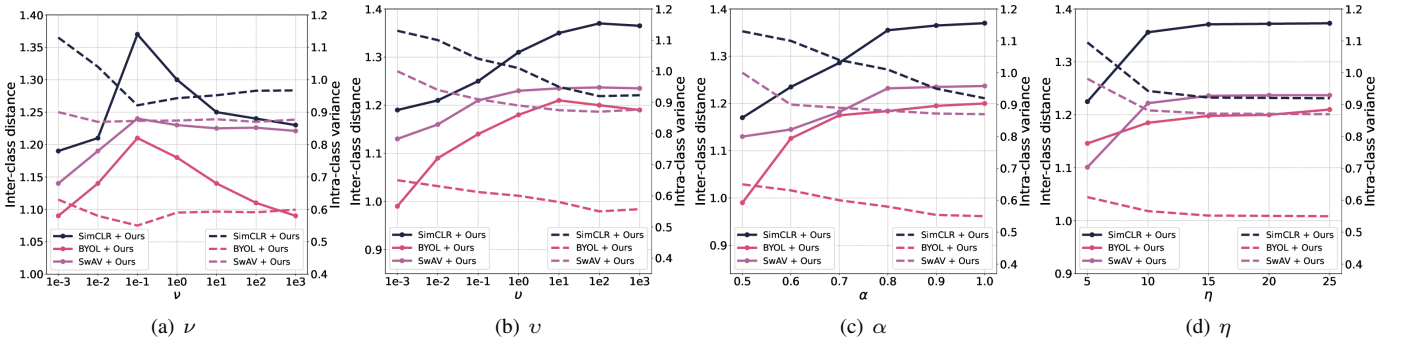


Fig. 4. The inter-class distance and intra-class variance correspond to different values of hyper-parameters ν , v , α , and η . The solid lines in figures (a) - (d) represent the inter-class distance while the dashed lines represent the intra-class variance.

TABLE IX

THE INTER-CLASS DISTANCE, THE INTRA-CLASS VARIANCE, AND THE LINEAR EVALUATION ACCURACY OF SIMCLR + DSA WITHOUT INDIVIDUAL COMPONENTS.

Method	Inter-class Dist. (\uparrow)	Intra-class Var. (\downarrow)	ACC (%)
SimCLR	1.17	1.15	70.15
+ DSA	1.37	0.92	72.09
+ DSA without SM	1.24	1.06	71.06
+ DSA without $sc(\cdot)$	1.32	0.97	71.67
BYOL	0.90	0.65	71.48
+ DSA	1.21	0.55	74.95
+ DSA without SM	0.96	0.63	72.13
+ DSA without $sc(\cdot)$	1.16	0.52	73.74
SwAV	1.12	1.01	75.78
+ DSA	1.31	0.57	77.84
+ DSA without SM	1.17	0.92	76.06
+ DSA without $sc(\cdot)$	1.26	0.67	77.23

E. Discriminant analysis

a) *Visualization of SSL features:* To validate the effectiveness of DSA, we used the same experimental setup as in Section IV-A. We visualized the representations obtained from self-supervised learning with DSA on the ImageNet test set using t-SNE. The feature visualization is shown in Figure 3. From the figure, it can be observed that after incorporating DSA, there are clear boundaries between clusters of different categories, and the distribution within the same category is more concentrated. Specifically, the t-SNE map of MAE + DSA in Figure 3(e) shows clustering characteristics compared to MAE in Figure 1(e). This indicates that the DSA algorithm effectively reduces intra-class variance and increases inter-class distance. In the next section, we further demonstrate this through quantitative experiments.

b) *Quantified evidence of discrimination:* We further conducted a quantitative analysis of DSA's intra-class variance and inter-class distance using the same methods as in Section IV-A. The results are presented in Table VIII.

From the table, it can be observed that for all SSL methods, the inclusion of DSA results in a reduction in intra-class variance and an increase in inter-class distance. This demonstrates the effectiveness of DSA. Additionally, as evidenced by the performance across various downstream tasks discussed in Section VI-D, reducing intra-class variance and increasing inter-class distance indeed enhance generalization. This validates the correctness of our theoretical analysis.

F. Ablation Study

a) *Analysis of Hyperparameters:* We explore the effects of hyperparameters ν , v , η , and α by showing the corresponding change of mean inter-class distance and intra-class variance with these hyperparameters. Specifically, ν represents the weight of \mathcal{L}_{AM}^s , v represents the weight of \mathcal{L}_{con} , η represents the number of nearest neighbors, α is a threshold in \mathcal{L}_{AM} . The results are illustrated in Figure 4. For results in 4(a) to 4(d), the results are obtained by fixing other hyperparameters while changing the corresponding hyperparameter.

From Figures 4(a) and 4(b), we can observe that in the objective function in Equation 17, the optimal weights for \mathcal{L}_{AM}^s and \mathcal{L}_{con} are achieved at $\nu = 1 \times 10^{-1}$ and $v = 1 \times 10^2$, respectively. From Figure 4(c), it can be seen that as α increases, the inter-class distance gradually rises and then stabilizes, while the intra-class variance continuously decreases and stabilizes. This result indicates that the score values output by the f_s

network can indeed measure the distance between samples. From Figure 4(d), we observe that as η increases, both the inter-class distance and intra-class variance experience significant growth from $\eta = 5$ to $\eta = 10$ and then level off. This suggests that when the number of nearest neighbor samples is small, the score $sc(z_i)$ obtained is not accurate. However, as η increases, the score $sc(z_i)$ becomes more accurate but stabilizes once η reaches a certain value. Therefore, the default value for η is set to 20.

b) *Ablation study on components of DSA*: We present an ablation study comparing different components of DSA, i.e. the SM and the scoring mechanism $sc(\cdot)$, in Table IX. Table IX shows inter-class distance, intra-class variance, and top-1 test accuracy on ImageNet for DSA without each individual component.

From Table IX, it can be seen that without incorporating SM, the inter-class distance is slightly higher than that of the original SSL method, and the final accuracy is also marginally higher than the original SSL method. This indicates that SM has a significant impact on the effectiveness of DSA. Moreover, even without $sc(\cdot)$, the performance is already significantly better than the original SSL method, though still lower than the full DSA method. This demonstrates that the weights obtained by sc play an important auxiliary role in the DSA method.

c) *The selection of f_{aux} and f_s* : To evaluate the impact of different choices of f_{aux} and f_s , we conduct ablation studies on the ImageNet test set. The default feature extractor is the pre-trained CLIP image encoder [63]. We evaluate the selection of f_{aux} with three other different feature extractors, namely open-source pre-trained ResNet-18, Scale-invariant feature transform (SIFT) [64], and BEiT [16]. The default setting for f_s is a two-layer MLP with ReLU activation function, we conduct experiments by substituting the network f_s with cosine similarity, which yields $M_{i,j} = \text{sim}(z_i, z_j) = \frac{z_i \cdot z_j^T}{\|z_i\| \|z_j\|}$. All results are depicted in Table X. From the results of f_{aux} , we can conclude that the performance of DSA is not impacted by the choice of pre-trained feature extractor (i.e., the architecture, pre-training method, or data), while the use of a pre-trained feature extractor is essential. The results of f_s demonstrate that the performance of cosine similarity deteriorates significantly compared to learnable MLP, thereby highlighting the efficacy of f_s .

TABLE X

TOP-1 ACCURACIES ON IMAGENET TEST SET FOR DIFFERENT SELECTION OF f_{aux} AND f_s

Network	Selection	Top-1 ACC (%)		
		SimCLR + DSA	BYOL + DSA	Barlow Twins + DSA
f_{aux}	CLIP	72.09	74.95	76.03
	BEiT	72.04	74.87	75.94
	SIFT	71.98	74.82	75.91
	ResNet-18	72.06	74.49	76.04
f_s	MLP	72.09	74.95	76.03
	Cosine Similarity	70.96	73.39	75.88

VII. CONCLUSION

In this paper, we present empirical evidence of the existence of the crowding problem in self-supervised learning and provide

theoretical proof that minimizing intra-class variance and maximizing inter-class separation effectively compresses the upper bound of classification error. Based on these findings, we propose a novel approach called "Dynamic Semantic Adjuster" (DSA), which aims to attract samples with similar semantics while repelling others. We evaluate the effectiveness of our proposed methods through experiments in comprehensive downstream tasks. We also provide visualization and quantified evidence to analyze the discriminability of the learned representation. The experimental results and ablation study demonstrate the effectiveness of our proposed DSA.

REFERENCES

- [1] T. Chen, S. Kornblith, M. Norouzi, and G. Hinton, "A Simple Framework for Contrastive Learning of Visual Representations," in *Proceedings of the 37th International Conference on Machine Learning*. PMLR, Nov. 2020, pp. 1597–1607.
- [2] J.-B. Grill, F. Strub, F. Althé, C. Tallec, P. Richemond, E. Buchatskaya, C. Doersch, B. Avila Pires, Z. Guo, M. Gheshlaghi Azar, B. Piot, k. kavukcuoglu, R. Munos, and M. Valko, "Bootstrap Your Own Latent - A New Approach to Self-Supervised Learning," in *Advances in Neural Information Processing Systems*, vol. 33. Curran Associates, Inc., 2020, pp. 21 271–21 284.
- [3] J. Zbontar, L. Jing, I. Misra, Y. LeCun, and S. Deny, "Barlow Twins: Self-Supervised Learning via Redundancy Reduction," in *Proceedings of the 38th International Conference on Machine Learning*. PMLR, Jul. 2021, pp. 12 310–12 320.
- [4] W. Qiang, J. Li, C. Zheng, B. Su, and H. Xiong, "Robust local preserving and global aligning network for adversarial domain adaptation," *IEEE Transactions on Knowledge and Data Engineering*, 2021.
- [5] J. Li, W. Qiang, C. Zheng, B. Su, F. Razzak, J.-R. Wen, and H. Xiong, "Modeling multiple views via implicitly preserving global consistency and local complementarity," *IEEE Transactions on Knowledge and Data Engineering*, 2022.
- [6] M. Caron, H. Touvron, I. Misra, H. Jégou, J. Mairal, P. Bojanowski, and A. Joulin, "Emerging properties in self-supervised vision transformers," in *Proceedings of the IEEE/CVF international conference on computer vision*, 2021, pp. 9650–9660.
- [7] A. Bardes, J. Ponce, and Y. LeCun, "Vicreg: Variance-invariance-covariance regularization for self-supervised learning," in *International Conference on Learning Representations*, 2021.
- [8] K. He, X. Chen, S. Xie, Y. Li, P. Dollár, and R. Girshick, "Masked autoencoders are scalable vision learners," in *Proceedings of the IEEE/CVF conference on computer vision and pattern recognition*, 2022, pp. 16 000–16 009.
- [9] Z. Xie, Z. Zhang, Y. Cao, Y. Lin, J. Bao, Z. Yao, Q. Dai, and H. Hu, "Simmim: A simple framework for masked image modeling," in *Proceedings of the IEEE/CVF conference on computer vision and pattern recognition*, 2022, pp. 9653–9663.
- [10] M. Caron, I. Misra, J. Mairal, P. Goyal, P. Bojanowski, and A. Joulin, "Unsupervised learning of visual features by contrasting cluster assignments," *Advances in Neural Information Processing Systems*, vol. 33, pp. 9912–9924, 2020.
- [11] J. Deng, W. Dong, R. Socher, L.-J. Li, K. Li, and L. Fei-Fei, "ImageNet: A large-scale hierarchical image database," in *2009 IEEE Conference on Computer Vision and Pattern Recognition*, Jun. 2009, pp. 248–255.
- [12] Y. Tian, D. Krishnan, and P. Isola, "Contrastive Multiview Coding," Dec. 2020.
- [13] X. Chen and K. He, "Exploring Simple Siamese Representation Learning," in *Proceedings of the IEEE/CVF Conference on Computer Vision and Pattern Recognition*, 2021, pp. 15 750–15 758.
- [14] A. Ermolov, A. Siarohin, E. Sangineto, and N. Sebe, "Whitening for self-supervised representation learning," in *International Conference on Machine Learning*. PMLR, 2021, pp. 3015–3024.
- [15] T. N. Kipf and M. Welling, "Variational graph auto-encoders," *arXiv preprint arXiv:1611.07308*, 2016.
- [16] H. Bao, L. Dong, S. Piao, and F. Wei, "Beit: Bert pre-training of image transformers," *arXiv preprint arXiv:2106.08254*, 2021.
- [17] S. Balakrishnama and A. Ganapathiraju, "Linear discriminant analysis-a brief tutorial," *Institute for Signal and information Processing*, vol. 18, no. 1998, pp. 1–8, 1998.

- [18] N. Saunshi, O. Plevrakis, S. Arora, M. Khodak, and H. Khandeparkar, "A Theoretical Analysis of Contrastive Unsupervised Representation Learning," in *Proceedings of the 36th International Conference on Machine Learning*. PMLR, May 2019, pp. 5628–5637.
- [19] S. Chen, C. Gong, J. Li, J. Yang, G. Niu, and M. Sugiyama, "Learning contrastive embedding in low-dimensional space," *Advances in Neural Information Processing Systems*, vol. 35, pp. 6345–6357, 2022.
- [20] C. M. Bishop, "Pattern recognition and machine learning," *Springer google schola*, vol. 2, pp. 1122–1128, 2006.
- [21] J. Yang, D. Parikh, and D. Batra, "Joint unsupervised learning of deep representations and image clusters," in *Proceedings of the IEEE conference on computer vision and pattern recognition*, 2016, pp. 5147–5156.
- [22] J. Xie, R. Girshick, and A. Farhadi, "Unsupervised deep embedding for clustering analysis," in *International conference on machine learning*. PMLR, 2016, pp. 478–487.
- [23] M. Caron, P. Bojanowski, A. Joulin, and M. Douze, "Deep clustering for unsupervised learning of visual features," in *Proceedings of the European conference on computer vision (ECCV)*, 2018, pp. 132–149.
- [24] J. Li, P. Zhou, C. Xiong, and S. C. H. Hoi, "Prototypical Contrastive Learning of Unsupervised Representations," Mar. 2021.
- [25] C.-Y. Ko, J. Mohapatra, S. Liu, P.-Y. Chen, L. Daniel, and L. Weng, "Revisiting contrastive learning through the lens of neighborhood component analysis: An integrated framework," in *International Conference on Machine Learning*. PMLR, 2022, pp. 11 387–11 412.
- [26] T. Wang and P. Isola, "Understanding contrastive representation learning through alignment and uniformity on the hypersphere," in *International Conference on Machine Learning*. PMLR, 2020, pp. 9929–9939.
- [27] J. Zhou, C. Wei, H. Wang, W. Shen, C. Xie, A. Yuille, and T. Kong, "ibot: Image bert pre-training with online tokenizer," *arXiv preprint arXiv:2111.07832*, 2021.
- [28] Q. Zhang, Y. Wang, and Y. Wang, "How mask matters: Towards theoretical understandings of masked autoencoders," *Advances in Neural Information Processing Systems*, vol. 35, pp. 27 127–27 139, 2022.
- [29] K. He, X. Zhang, S. Ren, and J. Sun, "Deep residual learning for image recognition," in *Proceedings of the IEEE Conference on Computer Vision and Pattern Recognition*, 2016, pp. 770–778.
- [30] A. Dosovitskiy, L. Beyer, A. Kolesnikov, D. Weissenborn, X. Zhai, T. Unterthiner, M. Dehghani, M. Minderer, G. Heigold, S. Gelly et al., "An image is worth 16x16 words: Transformers for image recognition at scale," *arXiv preprint arXiv:2010.11929*, 2020.
- [31] L. Van der Maaten and G. Hinton, "Visualizing data using t-sne," *Journal of machine learning research*, vol. 9, no. 11, 2008.
- [32] Y.-X. Wang, H. Xu, and C. Leng, "Provable subspace clustering: When lrr meets ssc," *Advances in Neural Information Processing Systems*, vol. 26, 2013.
- [33] W. Kay, J. Carreira, K. Simonyan, B. Zhang, C. Hillier, S. Vijayarasmihan, F. Viola, T. Green, T. Back, P. Natshe et al., "The kinetics human action video dataset," *arXiv preprint arXiv:1705.06950*, 2017.
- [34] T.-Y. Lin, M. Maire, S. Belongie, J. Hays, P. Perona, D. Ramanan, P. Dollár, and C. L. Zitnick, "Microsoft coco: Common objects in context," in *European conference on computer vision*. Springer, 2014, pp. 740–755.
- [35] M. Everingham, L. Van Gool, C. K. Williams, J. Winn, and A. Zisserman, "The pascal visual object classes (voc) challenge," *International journal of computer vision*, vol. 88, no. 2, pp. 303–338, 2010.
- [36] B. Oreshkin, P. Rodríguez López, and A. Lacoste, "Tadam: Task dependent adaptive metric for improved few-shot learning," *Advances in neural information processing systems*, vol. 31, 2018.
- [37] C. Wah, S. Branson, P. Welinder, P. Perona, and S. Belongie, "The caltech-ucsd birds-200-2011 dataset," 2011.
- [38] S. P. Mohanty, D. P. Hughes, and M. Salathé, "Using deep learning for image-based plant disease detection," *Frontiers in plant science*, vol. 7, p. 1419, 2016.
- [39] A. Krizhevsky and G. Hinton, "Learning multiple layers of features from tiny images," 2009.
- [40] I. Susmelj, M. Heller, P. Wirth, J. Prescott, and M. E. et al., "Lightly," GitHub. Note: <https://github.com/lightly-ai/lightly>, 2020.
- [41] C. Feichtenhofer, H. Fan, B. Xiong, R. Girshick, and K. He, "A Large-Scale Study on Unsupervised Spatiotemporal Representation Learning," Apr. 2021.
- [42] S. Ji, W. Xu, M. Yang, and K. Yu, "3d convolutional neural networks for human action recognition," *IEEE transactions on pattern analysis and machine intelligence*, vol. 35, no. 1, pp. 221–231, 2012.
- [43] C. Feichtenhofer, H. Fan, J. Malik, and K. He, "SlowFast Networks for Video Recognition," Oct. 2019.
- [44] K. He, H. Fan, Y. Wu, S. Xie, and R. Girshick, "Momentum Contrast for Unsupervised Visual Representation Learning," in *Proceedings of the IEEE/CVF Conference on Computer Vision and Pattern Recognition*, 2020, pp. 9729–9738.
- [45] N. Tomasev, I. Bica, B. McWilliams, L. Buesing, R. Pascanu, C. Blundell, and J. Mitrovic, "Pushing the limits of self-supervised resnets: Can we outperform supervised learning without labels on imagenet?" *arXiv preprint arXiv:2201.05119*, 2022.
- [46] S. Chen, G. Niu, C. Gong, J. Li, J. Yang, and M. Sugiyama, "Large-margin contrastive learning with distance polarization regularizer," in *International Conference on Machine Learning*. PMLR, 2021, pp. 1673–1683.
- [47] M. Zheng, S. You, F. Wang, C. Qian, C. Zhang, X. Wang, and C. Xu, "Ressl: Relational self-supervised learning with weak augmentation," *Advances in Neural Information Processing Systems*, vol. 34, pp. 2543–2555, 2021.
- [48] Y. Li, R. Pogodin, D. J. Sutherland, and A. Gretton, "Self-supervised learning with kernel dependence maximization," *Advances in Neural Information Processing Systems*, vol. 34, pp. 15 543–15 556, 2021.
- [49] S. Ozsoy, S. Hamdan, S. Arik, D. Yuret, and A. Erdogan, "Self-supervised learning with an information maximization criterion," *Advances in Neural Information Processing Systems*, vol. 35, pp. 35 240–35 253, 2022.
- [50] X. Liu, Z. Wang, Y.-L. Li, and S. Wang, "Self-supervised learning via maximum entropy coding," *Advances in Neural Information Processing Systems*, vol. 35, pp. 34 091–34 105, 2022.
- [51] A. Bardes, J. Ponce, and Y. LeCun, "Vicregl: Self-supervised learning of local visual features," *arXiv preprint arXiv:2210.01571*, 2022.
- [52] X. Chen, S. Xie, and K. He, "An empirical study of training self-supervised vision transformers," in *Proceedings of the IEEE/CVF international conference on computer vision*, 2021, pp. 9640–9649.
- [53] C. Yang, Y. Xu, B. Dai, and B. Zhou, "Video Representation Learning with Visual Tempo Consistency," Dec. 2020.
- [54] I. Dave, R. Gupta, M. N. Rizve, and M. Shah, "TCLR: Temporal Contrastive Learning for Video Representation," *Computer Vision and Image Understanding*, vol. 219, p. 103406, Jun. 2022, arXiv:2101.07974 [cs].
- [55] T. Pan, Y. Song, T. Yang, W. Jiang, and W. Liu, "Videomoco: Contrastive video representation learning with temporally adversarial examples," in *Proceedings of the IEEE/CVF conference on computer vision and pattern recognition*, 2021, pp. 11 205–11 214.
- [56] S. H. Khorasgani, Y. Chen, and F. Shkurti, "Slic: Self-supervised learning with iterative clustering for human action videos," in *Proceedings of the IEEE/CVF Conference on Computer Vision and Pattern Recognition*, 2022, pp. 16 091–16 101.
- [57] F. Xiao, J. Tighe, and D. Modolo, "Maclr: Motion-aware contrastive learning of representations for videos," in *European Conference on Computer Vision*. Springer, 2022, pp. 353–370.
- [58] R. Qian, T. Meng, B. Gong, M.-H. Yang, H. Wang, S. Belongie, and Y. Cui, "Spatiotemporal Contrastive Video Representation Learning," Apr. 2021.
- [59] H. Lee, K. Lee, K. Lee, H. Lee, and J. Shin, "Improving transferability of representations via augmentation-aware self-supervision," *Advances in Neural Information Processing Systems*, vol. 34, pp. 17 710–17 722, 2021.
- [60] W.-Y. Chen, Y.-C. Liu, Z. Kira, Y.-C. F. Wang, and J.-B. Huang, "A closer look at few-shot classification," in *International Conference on Learning Representations*, 2019.
- [61] S. Ren, K. He, R. Girshick, and J. Sun, "Faster r-cnn: Towards real-time object detection with region proposal networks," *Advances in neural information processing systems*, vol. 28, 2015.
- [62] K. He, G. Gkioxari, P. Dollár, and R. Girshick, "Mask r-cnn," in *Proceedings of the IEEE international conference on computer vision*, 2017, pp. 2961–2969.
- [63] A. Radford, J. W. Kim, C. Hallacy, A. Ramesh, G. Goh, S. Agarwal, G. Sastry, A. Askell, P. Mishkin, J. Clark et al., "Learning transferable visual models from natural language supervision," in *International Conference on Machine Learning*. PMLR, 2021, pp. 8748–8763.
- [64] D. G. Lowe, "Distinctive image features from scale-invariant keypoints," *International journal of computer vision*, vol. 60, pp. 91–110, 2004.

APPENDIX

A. Proofs

Theorem . IV.1. *If Assumption IV.1 holds, then, for any $f \in \mathcal{F}$, $\mathcal{L}_{CE}^\mu(f)$ can be bounded by $\mathcal{L}_{NCE}^\mu(f)$ as:*

$$\begin{aligned} \mathcal{L}_{CE}^\mu(f) \leq & \mathcal{L}_{NCE}(f) - \text{const} + \sum_{i=1, j=1, i \neq j}^K \mu_i^\top \mu_j \\ & + \sqrt{\text{Var}(f(x)|y)} + O(\text{const}^{-1/2}) \end{aligned} \quad (18)$$

where const is a constant that is related to the number of negative samples, $\mu_i = \mathbb{E}_{p(x|i)}[f(x)]$, and $\text{Var}(f(x)|y) = \mathbb{E}_{p(y)}[\mathbb{E}_{p(x|y)}\|f(x) - \mathbb{E}_{p(x|y)}f(x)\|^2]$.

Proof. Suppose that Q represents the number of negative samples. Then, we have:

$$\begin{aligned} & \mathbb{E}_{p(x_i, x_j)} \left[\log \frac{1}{Q} \sum_{i=1}^Q \exp(f^\top(x_i) f(x_j)) \right. \\ & \quad \left. - \log \mathbb{E}_{p(x_i)} \exp(f^\top(x_i) f(x_j)) \right] \\ & \leq e \mathbb{E}_{p(x_i, x_j)} \left[\frac{1}{Q} \sum_{i=1}^Q \exp(f^\top(x_i) f(x_j)) \right. \\ & \quad \left. - \mathbb{E}_{p(x_i)} \exp(f^\top(x_i) f(x_j)) \right] \\ & = \mathcal{O}\left(Q^{-\frac{1}{2}}\right) \end{aligned} \quad (19)$$

where the first inequality follows the Intermediate Value Theorem and e (the natural number) is the upper bound of the absolute derivative of \log between two points when $|f^\top(x_i) f(x_j)| \leq 1$. The second inequality follows the Berry-Esseen Theorem given the bounded support of $\exp(f^\top(x_i) f(x_j))$ as following: for i.i.d random variables ψ_i with bounded support $\text{supp}(\psi) \subset [-a, a]$, zero mean and bounded variance $\sigma_\psi^2 < a^2$, we have:

$$\begin{aligned} \mathbb{E} \left[\frac{1}{Q} \sum_{i=1}^Q \psi_i \right] &= \frac{\sigma_\psi}{\sqrt{Q}} \int_0^{\frac{a\sqrt{Q}}{\sigma_\psi}} p \left[\frac{1}{\sigma_\psi \sqrt{Q}} \sum_{i=1}^Q \psi_i > x \right] dx \\ &\leq \frac{\sigma_\psi}{\sqrt{Q}} \int_0^{\frac{a\sqrt{Q}}{\sigma_\psi}} p[|N(0, 1)| > x] dx + \frac{C_a}{\sqrt{Q}} \\ &\leq \frac{C_a}{\sqrt{Q}} + \frac{a}{\sqrt{Q}} \mathbb{E}[N(0, 1)] \\ &= \mathcal{O}\left(Q^{-\frac{1}{2}}\right) \end{aligned} \quad (20)$$

where C_a is the constant that only depends on a and $\psi_i = \exp(f^\top(x_i) f(x_j))$.

Then, we suppose that the classification task consists of K categories and denote that u_y as the center of features of class y , $y \in \{1, \dots, K\}$. We denote $p(x, x^+, y)$ as the joint distribution of the positive pairs x, x^+, y , denote x^+ as the random variable of positive sample, denote x_i^+ as a negative sample, denote x^- as the random variable of negative sample, and denote y^- as the negative class. We have:

$$\begin{aligned} \mathcal{L}_{NCE} &= -\mathbb{E}_{p(x, x^+)} f(x)^\top f(x^+) \\ &+ \mathbb{E}_{p(x)} \mathbb{E}_{p(x_i^-)} \log \sum_{i=1}^Q \exp(f(x)^\top f(x_i^-)) + \log Q \\ &\geq -\mathbb{E}_{p(x, x^+)} f(x)^\top f(x^+) \\ &+ \mathbb{E}_{p(x)} \log \frac{1}{Q} \mathbb{E}_{p(x_i^-)} \exp(f(x)^\top f(x_i^-)) + \log Q \\ &\geq -\mathbb{E}_{p(x, x^+, y)} f(x)^\top f(x^+) - \text{const}(Q) + \log Q \\ &+ \mathbb{E}_{p(x)} \log \frac{1}{Q} \mathbb{E}_{p(y^-)} \mathbb{E}_{p(x_i^-|y^-)} \exp(f(x)^\top f(x_i^-)) \\ &\geq -\mathbb{E}_{p(x, x^+, y)} [f(x)^\top u_y + \|f(x^+) - u_y\|] \\ &+ \mathbb{E}_{p(x)} \log \mathbb{E}_{p(y^-)} \exp(f(x)^\top u_{y^-}) \\ &- \text{const}(Q) + \log Q - \sum_{i=1, j=1, i \neq j}^K \mu_i^\top \mu_j \\ &\geq -\mathbb{E}_{p(x, y)} f(x)^\top u_y - \sqrt{\mathbb{E}_{p(x, y)} \|f(x) - u_y\|^2} \\ &+ \mathbb{E}_{p(x)} \log \mathbb{E}_{p(y^-)} \exp(f(x)^\top u_{y^-}) \\ &- \text{const}(Q) + \log Q - \sum_{i=1, j=1, i \neq j}^K \mu_i^\top \mu_j \\ &= \mathbb{E}_{p(x, y)} [-f(x)^\top u_y + \log \sum_{k=1}^K \exp(f(x)^\top u_k)] + \log M \\ &- \sqrt{\text{Var}(f(x)|y)} - \text{const}(Q) - \sum_{i=1, j=1, i \neq j}^K \mu_i^\top \mu_j \\ &= \mathcal{L}_{CE}^\mu(f) - \sqrt{\text{Var}(f(x)|y)} - \text{const}(Q) \\ &+ \log \frac{Q}{K} - \sum_{i=1, j=1, i \neq j}^K \mu_i^\top \mu_j \\ &= \mathcal{L}_{CE}^\mu(f) - \sqrt{\text{Var}(f(x)|y)} - \sum_{i=1, j=1, i \neq j}^K \mu_i^\top \mu_j \\ &+ \mathcal{O}(\text{const}(Q)^{-\frac{1}{2}}) \end{aligned} \quad (21)$$

□